Biomechanics and Modeling in Mechanobiology

GLENOHUMERAL JOINT RECONSTRUCTION USING STATISTICAL SHAPE MODELING

--Manuscript Draft--

Manuscript Number:	
Full Title:	GLENOHUMERAL JOINT RECONSTRUCTION USING STATISTICAL SHAPE MODELING
Article Type:	Original Research
Keywords:	statistical shape model; shoulder joint; biomechanical model; surgical planning; humerus; scapula
Corresponding Author:	David Ackland University of Melbourne AUSTRALIA
Corresponding Author Secondary Information:	
Corresponding Author's Institution:	University of Melbourne
Corresponding Author's Secondary Institution:	
First Author:	Yichen Huang, BSc, MEng
First Author Secondary Information:	
Order of Authors:	Yichen Huang, BSc, MEng
	Dale L Robinson, PhD
	Jonathan Pitocchi, PhD
	Peter Vee Sin Lee, PhD
	David Ackland, PhD
Order of Authors Secondary Information:	
Funding Information:	Australian Research Council Future Fellowship (FT200100098) — A/Prof David Ackland
	Australian Research Council Industry Transformation Training Centre (IC180100024) — Prof Peter Vee Sin Lee
Abstract:	Evaluation of the bony anatomy of the glenohumeral joint is frequently required for surgical planning and subject-specific computational modelling and simulation. The three-dimensional geometry of bones is traditionally obtained by segmenting medical image datasets, but this can be time-consuming and is usually not practical in the clinical setting. The aims of this study were twofold. Firstly, to develop and validate a statistical shape modeling approach to rapidly reconstruct the complete scapular and humeral geometries using discrete morphometric measurements that can be quickly and easily measured directly from CT, and secondly, to assess the effectiveness of statistical shape modeling in reconstruction of the entire humerus long-bone using just the landmarks in the immediate vicinity of the glenohumeral joint. The most representative shape prediction models presented in this study achieved complete scapular and humeral geometry prediction from seven or fewer morphometric measurements and yielded a mean surface root mean square (RMS) error under 2 mm. Reconstruction of the entire humerus was achieved using information of only proximal humerus bony landmarks and yielding mean surface RMS errors under 3 mm. The proposed statistical shape modelling facilitates rapid generation of 3D anatomical models of the glenohumeral joint, which may be useful in rapid development of personalized musculoskeletal models.

GLENOHUMERAL JOINT RECONSTRUCTION USING STATISTICAL SHAPE MODELING

[1]Yichen Huang, [1]Dale L. Robinson, [2]Jonathan Pitocchi, [1]Peter Vee Sin Lee, [1]David C. Ackland

[1]Department of Biomedical Engineering, University of Melbourne, Parkville, Victoria 3010, AUSTRALIA; [2]Materialise, Heverlee, Belgium

Submitted as an original article to: *Biomechanics and Modeling in Mechanobiology*

Word count (Introduction to Discussion): 3,795

Address for correspondence:

David C. Ackland
Department of Biomedical Engineering
University of Melbourne
Parkville, Victoria 3010, AUSTRALIA
Phone: +613 8344 8646
Fax:
Email: dackland@unimelb.edu.au

Key Words: statistical shape model; shoulder joint; biomechanical model; surgical planning; humerus; scapula

ABSTRACT

Evaluation of the bony anatomy of the glenohumeral joint is frequently required for surgical planning and subject-specific computational modelling and simulation. The three-dimensional geometry of bones is traditionally obtained by segmenting medical image datasets, but this can be time-consuming and is usually not practical in the clinical setting. The aims of this study were twofold. Firstly, to develop and validate a statistical shape modeling approach to rapidly reconstruct the complete scapular and humeral geometries using discrete morphometric measurements that can be quickly and easily measured directly from CT, and secondly, to assess the effectiveness of statistical shape modeling in reconstruction of the entire humerus long-bone using just the landmarks in the immediate vicinity of the glenohumeral joint. The most representative shape prediction models presented in this study achieved complete scapular and humeral geometry prediction from seven or fewer morphometric measurements and yielded a mean surface root mean square (RMS) error under 2 mm. Reconstruction of the entire humerus was achieved using information of only proximal humerus bony landmarks and yielding mean surface RMS errors under 3 mm. The proposed statistical shape modelling facilitates rapid generation of 3D anatomical models of the glenohumeral joint, which may be useful in rapid development of personalized musculoskeletal models.

INTRODUCTION

The bony anatomy of the glenohumeral joint is known to vary significantly across the population, and is influenced by factors such as age, sex, and ethnicity (Sintini et al. 2018; von Schroeder 2001). The size and shape of the scapula and humerus influences the paths of muscle-tendon units spanning the glenohumeral joint, which affects their muscle moment arms, lines of action, the operating region on the force-length and force-velocity curves, and resultant muscle-generated joint forces (Raikova et al. 2001). Consequently, evaluation of the three-dimensional geometry of these bones has played an important role in subject-specific computational modelling and simulation at the shoulder, facilitating surgical planning, virtual clinical trials, implant design, and prescription of rehabilitation (Frankle et al. 2009; Pearl 2005).

The three-dimensional geometry of bones is traditionally obtained by segmenting image datasets derived from computed tomography (CT) or magnetic resonance imaging (MRI), but this can be time consuming and impractical for clinical settings. The scaling of generic bone surfaces is commonly employed as an alternative, including linear scaling based on bone anthropometric measurements, which can be performed rapidly and with high computational efficiency; however, this approach generally cannot be used to accurately discern subject-specific bone morphology and features such as muscle and ligament attachment (Scheys et al. 2008; Wu et al. 2016). Mean RMS errors in excess of 5 mm have been reported in predicting pelvis, femur, tibia, fibula, and patella geometry using linear scaling (Zhang et al. 2016a), with hip muscle moment arm errors of up to 16.7 mm (Bahl et al. 2019).

Statistical shape modelling of bones is a mathematical approach that has been used to describe bony features across a group or population using principal component analysis (PCA) (Jolliffe 1986). At the shoulder, statistical shape modeling has been used to identify sex and ethnicity differences in the cortical and cancellous proximal humerus (Sintini et al. 2018), assess morphologic and material property variations in the scapula (Burton et al. 2019; Casier et al. 2018), evaluate scapula cortical thickness across populations (Pitocchi et al. 2020), and reconstruct glenoid anatomy with RMS errors as low as 1.0 ± 0.2 mm (Abler et al. 2018). In addition, SSM has been used as a tool for reconstruction of complete bone geometry from a limited image dataset. For example, Zhang et al. (2016a) used SSM to predict entire surface geometry of the pelvis, femur, tibia, fibula, and patella from seven landmarks digitized using video motion-capture. They demonstrated a mean RMS error of the predicted shapes of 4.3 mm, which was an improvement over that of linear scaling methods (RMS error of 5.2 mm).

The ability to predict complete geometry of bones from a limited set of geometric measurements has application in rapid generation of subject-specific bone and joint models and may ultimately avoid the time-consuming process of image segmentation. At present, the predictability of scapular and humeral surface reconstruction using discrete bony landmarks remains poorly understood. This includes estimation of the entire humeral geometry using only bony features from the proximal humerus, which is most commonly acquired using CT for pre-operative planning of shoulder surgery. The aims of the present study were twofold. Firstly, to develop and validate a statistical shape modeling approach for rapid reconstruction of complete scapular and humeral geometries using a small number of clinically relevant morphometric measurements derived from CT; and secondly, to assess the effectiveness of statistical shape modeling in reconstruction of the entire humeral long bone using only morphometric measurements of bony landmarks in the immediate vicinity of the glenohumeral joint. The findings will have implications for rapid subject-specific shoulder model development using image datasets commonly acquired in the clinical setting.

METHODS

Statistical shape model generation

Right scapular geometries of thirty male (age 60.3±10.0 years, weight 72.1±10.9 kg) and thirty female subjects (age 58.1±8.7 years, weight 61.0±16.0 kg) together with right humeral geometries of thirty male (age 61.0±10.5 years, weight 64.6±10.3 kg) and thirty female subjects (age 58.6±10.2 years, weight 54.3±9.3 kg) were digitally reconstructed from CT scans using commercially available software (Mimics 21.0, Materialise NV, Belgium) (Table S1-S4, Supplementary Material). All subjects were head and neck cancer patients that were free of macroscopic shoulder bone abnormalities. The CT scans were obtained from a publicly accessible database (QIN-HEADNECK) and had a slice thickness of either 3 mm or 5 mm (Clark et al. 2013; Fedorov et al. 2016; R et al. 2015). Bone surfaces derived from the image segmentation were smoothed and re-meshed to produce surfaces with a nominal element size of 1.0 mm (Geomagic Wrap 2015, 3D Systems, USA). The resultant surface meshes were used as training sets for the generation of four statistical shape models (SSMs) representing the scapula and humerus for both males and females.

Generation of SSMs comprised (i) non-rigid registration, (ii) rigid body alignment and (iii) PCA. First, non-rigid registration was used to establish nodal correspondence among the training meshes. This was achieved by registering a template mesh of median size and shape using the first two principal components to all other meshes in the same training set using a radial basis function (RBF) non-rigid registration algorithm (Zhang et al. 2018).

A rigid body alignment algorithm was then applied to all registered meshes in the training set. This process, which eliminated variation caused by rotation and translation, was employed using an iterative closest point (ICP) algorithm that minimized the sum of squared distances between corresponding nodes of two shape surfaces (Besl and McKay 1992).

Finally, PCA was applied to each of the four training sets i.e., male scapula, female scapula, male humerus and female humerus, to achieve dimensionality reduction (Jolliffe 1986). PCA allowed any shape in the training set to be approximated as the mean shape plus a linear combination of the first *k* principal components

$$\boldsymbol{X} = \overline{\boldsymbol{X}} + \sum_{i=1}^{k} b_i \boldsymbol{\Phi}_i \quad (1)$$

where $\boldsymbol{X}$ represents a random shape in the training set, $\overline{\boldsymbol{X}}$ represents the mean shape, $\boldsymbol{\Phi}_i$ represents the *i*th principal component, and b_i represents the principal component score for $\boldsymbol{\Phi}_i$.

The software GIAS2, which is part of the MAP Client open-source platform (Zhang et al. 2014), was used to perform non-rigid registration and rigid body alignment when generating SSMs.

Morphometric measurements

Fifteen clinically relevant anatomical scapular landmarks (Table 1) and eight humeral landmarks adapted from previous studies (Table 2) (Arias-Martorell et al. 2014; Kranioti et al. 2009; Polguj et al. 2016; von Schroeder 2001) were manually identified on each scapular and humeral mesh (Fig. 1). These landmarks were also identified on the mean shape of each training set. The scalar distance between all combinations of two landmarks were then calculated for each scapula and humerus mesh (Matlab R2019b, MathWorks, USA). Landmarks of each training mesh were then registered to the landmarks of the corresponding mean shape mesh using singular value decomposition (SVD) to ensure that the variations in the 3-dimensional coordinates of each landmark were a consequence of geometric variations only. The registered landmark coordinates and the calculated scalar distances between landmarks were assembled into a measurement data matrix $\boldsymbol{m}$, which was used in subsequent analyses. For the humerus, the humeral head radius and the mid shaft girth were also included in the measurement data matrix $\boldsymbol{m}$ to better characterize the morphology of these regions (Chatterjee et al. 2017; DeLude et al. 2007).

Shape prediction

The scapula and humerus shape prediction models were built using a univariate least absolute shrinkage and selection operator (Lasso) regression (Tibshirani 1996). The principal component scores, b_i, of the first *k* principal components of a scapular or humeral mesh were predicted from an ensemble of Lasso regressors, *R*, using

$$\hat{b}_i = R_i(\boldsymbol{m}_i) \tag{2}$$

$$R = \{R_1, R_2, \dots, R_k\} \tag{3}$$

where $\hat{b}_i$ is the predicted principal component score for the *i*th principal component, R_i is the Lasso regressor for $\hat{b}_i$, and $\boldsymbol{m}_i \in \boldsymbol{m}$ is a subset of the measurement data matrix $\boldsymbol{m}$.

With the principal component scores of the first *k* principal components, the scapular and humeral meshes were then reconstructed using Eq. (1). Bayesian information criterion (BIC) was used to control the Lasso regression to select an optimal shape prediction model with good fit and reasonable complexity. This was achieved using an iterative process:

1. In the initial iteration, an ensemble of Lasso regressors R^0 was found from the whole measurement data matrix, $\boldsymbol{m}^0$.
2. In the ith iteration, any morphometric measurements not used or used by the least number of regressors in R^{i-1} were excluded from $\boldsymbol{m}^i$. If there existed a tie for the least used measurement, the measurement used in the regressor of the principal component score of the higher order principal component was dropped. R^i was then found using $\boldsymbol{m}^i$.

3. Step 2 was repeated until only 1 measurement was left.
4. For each iteration, the sum of BICs of the Lasso regressors in R^i was recorded. The optimal ensemble R^* was chosen as the ensemble that had the lowest sum of BICs.
5. The optimal number of principal components k^* was then selected by training ensembles $R^*_{k=2,4,6,8,10}$ and selecting the *k* that produce the smallest leave-one-out RMS error between the predicted and actual surface meshes.

For each of the four SSMs, the most representative shape prediction model was chosen as the one formed by the optimal ensemble, R^*, and the optimal number of principal components, k^*.

Since clinical CT scans of the glenohumeral joint typically exclude the distal humerus, such as those taken during surgical planning of shoulder arthroplasty, scapular and humeral shape predictions were evaluated using (i) all scapular and humeral morphometric measurements, and (ii) morphometric measurements derived from the proximal humerus only (Table 2).

Model validation

The capability of the SSMs to approximate shapes not used in model training was evaluated using a leave-one-out strategy. Specifically, each mesh within a given training set was predicted using the SSM derived from the corresponding training set less the given mesh. The predicted mesh was then compared to the actual mesh from CT image segmentation. Shape prediction accuracy was quantified using (i) surface RMS error, which was defined as the RMS distance between every point on the predicted mesh and its closest neighboring point on the actual mesh, and (ii) region- and landmark-specific RMS error, which was defined as the RMS distance calculated between every point on a specific region or landmark of the predicted mesh and its closest neighboring point on the actual mesh. Region- and landmark-specific RMS error was calculated using (i) the proximal humerus, defined as the region of the humerus proximal to the surgical neck of the humerus (ii) the glenoid, which was defined by the entire glenohumeral joint articular surface located on the lateral angle of the scapula, and (iii) each of the anatomical scapular and humeral landmarks used in the shape predictions (Fig. 1).

RESULTS

Scapular shape prediction using morphometric measurements

The first two principal components of the male scapula SSM produced the smallest mean surface RMS error (1.8 mm), thus the corresponding shape prediction model was considered the most representative shape prediction model for the male scapula (Fig. 2a). Similarly, the first eight principal components of the female scapula SSM were found to produce the smallest mean surface RMS error (1.6 mm), and the corresponding shape prediction model was the most representative shape prediction model for the female scapula (Fig. 2b).

Six morphometric measurements were required as inputs to achieve a mean surface RMS error of 1.8 mm in male scapula shape prediction, which included the scalar distances between scapular landmarks B and M, C and D, D and J, G and I, G and M as well as I and L. In contrast, seven morphometric measurements were required as inputs to achieve a mean surface RMS error of 1.6 mm in female scapula shape prediction, including the 3-dimensional coordinates of scapular landmarks L and M as well as the scalar distance between I and J. For the male and female scapulae, shape prediction error was largest (≥3.0 mm and ≥2.5 mm for male and female, respectively) on the inferior angle, superior angle, and tips of coracoid process and acromion, while the glenoid, scapular spine, supraspinous fossa, and infraspinous fossa yielded the lowest shape prediction error (≤2.0 mm) (Fig. 3a and Fig. 3b). Landmark A was the most poorly predicted landmark and had the highest mean RMS error (9.1 mm and 7.8

mm for male and female, respectively), while landmark E was best predicted with the lowest mean RMS error (2.7 mm and 2.6 mm for male and female, respectively) (Fig. 4a and Fig. 4b). The glenoid was generally well predicted in both cases, with a mean RMS error of 1.6 mm for both male and female glenoids.

Humeral shape prediction using morphometric measurements

The first two principal components of the male humerus SSM produced the smallest mean surface RMS error (1.6 mm), and the corresponding shape prediction model was considered the most representative shape prediction model for the male humerus (Fig. 2c). Similarly, the first eight principal components of the female humerus SSM produced the smallest mean surface RMS error (1.4 mm), and the corresponding shape prediction model was the most representative shape prediction model for the female humerus (Fig. 2d).

Seven morphometric measurements were required as inputs to achieve a mean surface RMS error of 1.6 mm in male humerus shape prediction, which included the 3-dimensional coordinates of humeral landmarks Q and T as well as the scalar distance between P and V. In contrast, six morphometric measurements were required as inputs to achieve a mean surface RMS error of 1.4 mm in female humerus shape prediction, specifically, the 3-dimensional coordinates of humeral landmarks P and Q. For the male humerus, shape prediction error was largest (≥2.0 mm) around the greater tubercle, lesser tubercle, and the lateral epicondyle, while for the female humerus, shape prediction error was largest (≥1.6 mm) around the superior and inferior-posterior regions of the humeral head as well as the inferior edge of the distal humerus (Fig. 3c and Fig. 3d). In both cases, the humeral shaft yielded the lowest shape prediction error (≤1.6 mm and ≤1.4 mm for male and female, respectively). For humeral landmarks, the highest mean RMS error was found at landmark R (6.0 mm and 4.8 mm for male and female, respectively), while the lowest mean RMS error was found at landmark U for male (3.6 mm) and landmark W for female (2.8 mm) (Fig. 4c and Fig. 4d). The mean RMS error of the proximal humerus was 1.8 mm and 1.4 mm for male and female, respectively.

Humeral shape prediction using proximal humerus morphometric measurements

The first four principal components of the male humerus SSM produced the smallest mean surface RMS error (2.7 mm), thus the corresponding shape prediction model was considered the most representative shape prediction model for the male humerus (Fig. 5a). Similarly, the first six principal components of the female humerus SSM produced the smallest mean surface RMS error (2.1 mm), and the corresponding shape prediction model was the most representative shape prediction model for the female humerus (Fig. 5b).

Four morphometric measurements were required as inputs to achieve a mean surface RMS error of 2.7 mm in male humerus shape prediction (scalar distances between P and R, P and S, Q and R as well as Q and S). For the female humerus, four morphometric measurements were required as inputs to achieve a mean surface RMS error of 2.1 mm in shape prediction, specifically, the 3-dimensional coordinates of humeral landmark Q and the humeral head radius. For male and female humeri, shape prediction error was found to be largest (≥5.0 mm and ≥3.5 mm for male and female, respectively) around the superior region of proximal humerus and the inferior edge of distal humerus (Fig. 6a and Fig. 6b), while the humeral shaft yielded the lowest shape prediction error (≤2.5 mm and ≤2.0 mm for male and female, respectively). For landmarks, the highest mean RMS error was found at landmark V (10.0 mm and 7.4 mm for male and female, respectively), while the lowest mean RMS error was found at landmark P for male (6.8 mm) and landmark Q for female (5.2 mm) (Fig. 7a and Fig. 7b). The proximal humerus was predicted with a mean RMS error of 3.0 mm and 2.5 mm for male and female proximal humeri, respectively.

DISCUSSION

This study presented a technique for reconstructing scapular and humeral bony geometry using statistical shape modeling and morphometric measurements that can be readily evaluated radiographically, thus avoiding time-consuming bone segmentation. The most representative shape prediction models presented in this study achieved a mean surface RMS error of 1.8 mm, 1.6 mm, 1.6 mm and 1.4 mm for male scapulae, female scapulae, male humeri and female humeri, respectively. These errors are substantially lower than that of the CT slice thickness used in model development (3.0-5.0 mm), and of similar magnitude as the accuracy of glenoid baseplate positioning in total shoulder arthroplasty using patient-specific instruments reported by Levy et al. (2014) (1.2±0.7 mm) and Hendel et al. (2012) (2.4±1.6 mm). In addition, the glenoid and the proximal humerus, which are regions of interest in shoulder imaging and surgical planning, were well predicted by the representative bone models with a mean RMS error of under 2 mm. This finding is comparable to the accuracy of the SSM-based glenoid reconstruction techniques described by Plessers et al. (2018) (RMS error of 1.2±0.4 mm) and Abler et al. (2018) (RMS error of 1.0±0.2 mm).

Region-specific RMS errors in scapular and humeral landmark prediction, which may be used as a surrogate measure of muscle attachment site estimation accuracy, yielded mean landmark RMS errors below 10 mm for all scapular landmarks and below 6 mm for all humeral landmarks. This compares favorably to the non-linear morphing method presented by Pellikaan et al. (2014) (69% of the muscle attachment sites with a mean error less than 15 mm) and Kaptein and van der Helm (2004) (45% of the muscle attachment sites with a mean error less than 7 mm), and is of similar magnitude as the humeral muscle attachment site estimation accuracy of a SSM-based method presented by Pitocchi et al. (2021) (median error less than 3.5 mm). However, a shortcoming of these previously techniques is that they require a segmented bone model as the registration target. The technique presented in this study enables rapid generation of patient-specific 3D models of the glenohumeral joint without the need of image segmentation, and is an improvement on standard linear scaling methods in both overall and region-specific bone geometry reconstruction accuracy.

Pre-operative CT scanning of the glenohumeral joint is commonly performed in surgical planning prior to arthroplasty (Scalise et al. 2008); however, the image datasets acquired typically exclude the distal humerus. Reconstruction of both the proximal and distal humerus is relevant in the estimating distal humerus muscle attachment sites, for example, in developing subject-specific musculoskeletal models of the upper limb, as well as in establishing the ISB recommended humeral joint coordinate system, which requires the epicondyle positions. We showed that accurate reconstruction of the entire humeral geometry is possible using only proximal humerus morphometric measurements with a mean surface RMS error of 2.7 mm and 2.1 mm for male and female humeri, respectively. The proximal humerus was reasonably well predicted, with a mean RMS error of 3.0 mm and 2.5 mm for male and female proximal humeri, respectively. This accuracy is higher than that reported for the proximal femur using a similar SSM approach by Zhang and Besier (2017) (RMS error of 10.4±3.2 mm), and is of the same order of magnitude to that reported by Hendel et al. (2012) for glenoid baseplate positioning in anatomic total shoulder arthroplasty (3.4±1.8 mm). In the present study, humeral landmark RMS errors were no larger than 10 mm, which is comparable to the muscle attachment site estimation accuracy of non-linear morphing methods (Kaptein and van der Helm 2004; Pellikaan et al. 2014). These findings suggest that segmentation of the entire humerus may be avoided in developing patient-specific anatomical models of this bone for normal adult subjects.

In the present study, shape prediction accuracies for male and female bones were found to be similar, with differences in mean surface RMS errors less than 1 mm. This finding is consistent with the fact that principal components of male and female SSMs are overall similar.

For example, the first three principal components of the SSMs of male and female scapulae, which accounted for more than 60% of the total shape variation, described virtually identically changes in scapula shape (Fig. S1, Supplementary Material). This result also supports the findings of previous studies that showed bony morphology of the glenohumeral joint of males and females is similar, though the male bone is typically larger in size (Sintini et al. 2018; Zhang et al. 2016b). In addition, we found no significant correlation was found between the number of principal components used in building shape prediction model and shape prediction accuracy. This is due to the fact that the first two principal components were most dominant, accounting for more than half of the total scapular shape variation and around 90% of the total humeral shape variation (Fig. S2, Supplementary Material). Including higher order principal components is likely to have little overall effect on shape prediction accuracy.

This study has a number of limitations that ought to be considered. First, the training sets used in this study only had thirty subjects for each gender, and the findings may not be generalized to very large cohorts. This training set size has been used in previous SSM studies (Vallabh et al. 2019; Zhang et al. 2016a), and our findings demonstrated subject-specific shoulder bone geometry reconstruction that is an improvement on linear scaling methods. Second, bone pathology was not explored in this study, and may ultimately affect SSMs and their capacity to predict shoulder geometry in the clinical setting. Future studies ought to evaluate the effects of bone pathologies on the morphology of the glenohumeral joint and shape prediction effectiveness using the SSM-based approaches. Finally, this study used clinically relevant landmark coordinates and scalar distance measurements for the scapula and humerus in shape prediction. Higher order principal components of the SSMs may be associated with twisting and rotating variations in bone shape, which were not explored (Fig. S1 and Fig. S3, Supplementary Material).

This study, which presented a SSM-based technique for reconstructing complete scapular and humeral anatomy from simple morphometric measurements, showed that between six and seven morphometric measurements are required to reconstruct complete scapular and humeral geometries with an accuracy that exceeds that of traditional linear scaling methods. Reconstruction of the entire humerus can be achieved using imaging data derived only for the proximal humerus, indicating that digitization of the entire long-bone may not be required in developing accurate patient-specific humeral bone models. The SSM-based technique presented in this study will facilitate rapid generation of 3D anatomical models of the scapula, humerus, and glenohumeral joint, which may be useful in patient-specific computational modelling and surgical planning.

COMPLIANCE WITH ETHICAL STANDARDS

The authors declare that they have no conflicts of interest

ACKNOWLEDGEMENTS

This project was funded by an Australian Research Council Industry Transformation Training Centre (IC180100024) and a Future Fellowship (FT200100098).

FIGURE CAPTIONS

Fig. 1 Scapular (a) and humeral landmarks (b) used in shape prediction. For descriptions of the landmarks, see Table 1 and Table 2

Fig. 2 Leave-one-out surface RMS error of male scapula (a), female scapula (b), male humerus (c), and female humerus (d) shape predictions from their corresponding ensembles $R^*_{k=2,4,6,8,10}$ derived using morphometric measurements calculated from the anatomical landmarks

Fig. 3 Error maps of the mean nodal error across the male scapula (a), female scapula (b), male humerus (c), and female humerus (d). Nodal errors were evaluated by comparing the predicted shape from the most representative bone model to the actual shape. The error at a given node was calculated by taking the mean nodal errors at the same node across all predicted shapes

Fig. 4 Leave-one-out region- and landmark-specific RMS error of the most representative models for male scapula (a), female scapula (b), male humerus (c) and female humerus (d). Region- and landmark-specific RMS error was calculated using the proximal humerus, glenoid of scapula and each of the anatomical scapular landmarks and anatomical humeral landmarks (see Table 1 and Table 2)

Fig. 5 Leave-one-out surface RMS errors for male humerus (a) and female humerus (b) shape predictions from their corresponding ensembles $R^*_{k=2,4,6,8,10}$ derived using only proximal humerus morphometric measurements

Fig. 6 Error maps of the mean nodal error across the male humerus (a) and female humerus (b) when comparing the predicted shape from the most representative bone models to actual shape. Only proximal humerus morphometric measurements were used

Fig. 7 Leave-one-out region- and landmark-specific RMS errors for the most representative models of the male humerus (a) and female humerus (b) derived using only proximal humerus morphometric measurements. Region- and landmark-specific RMS errors were calculated using the anatomical landmarks of the proximal humerus (see Table 2)

Figure 1

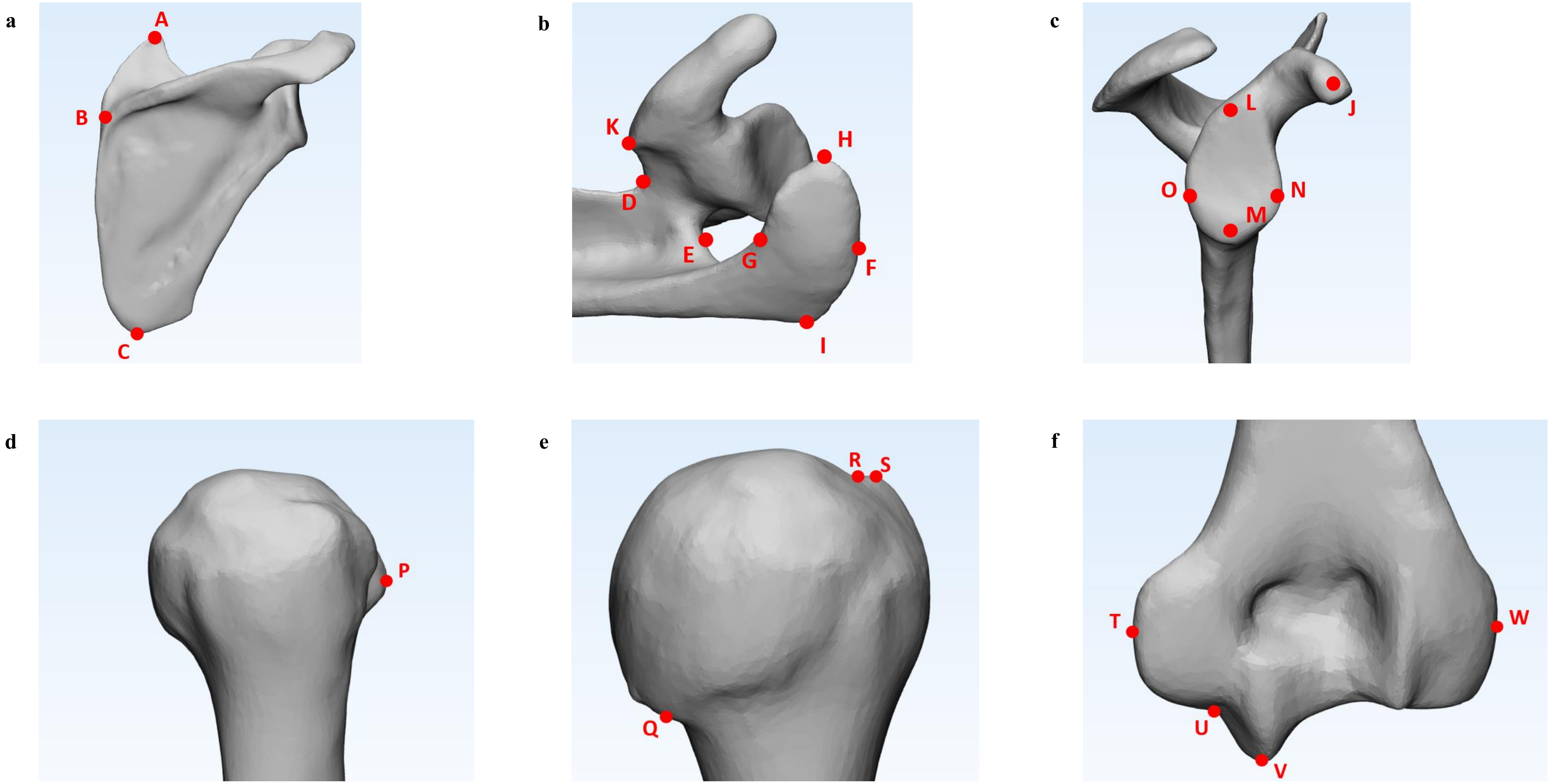

Figure 2

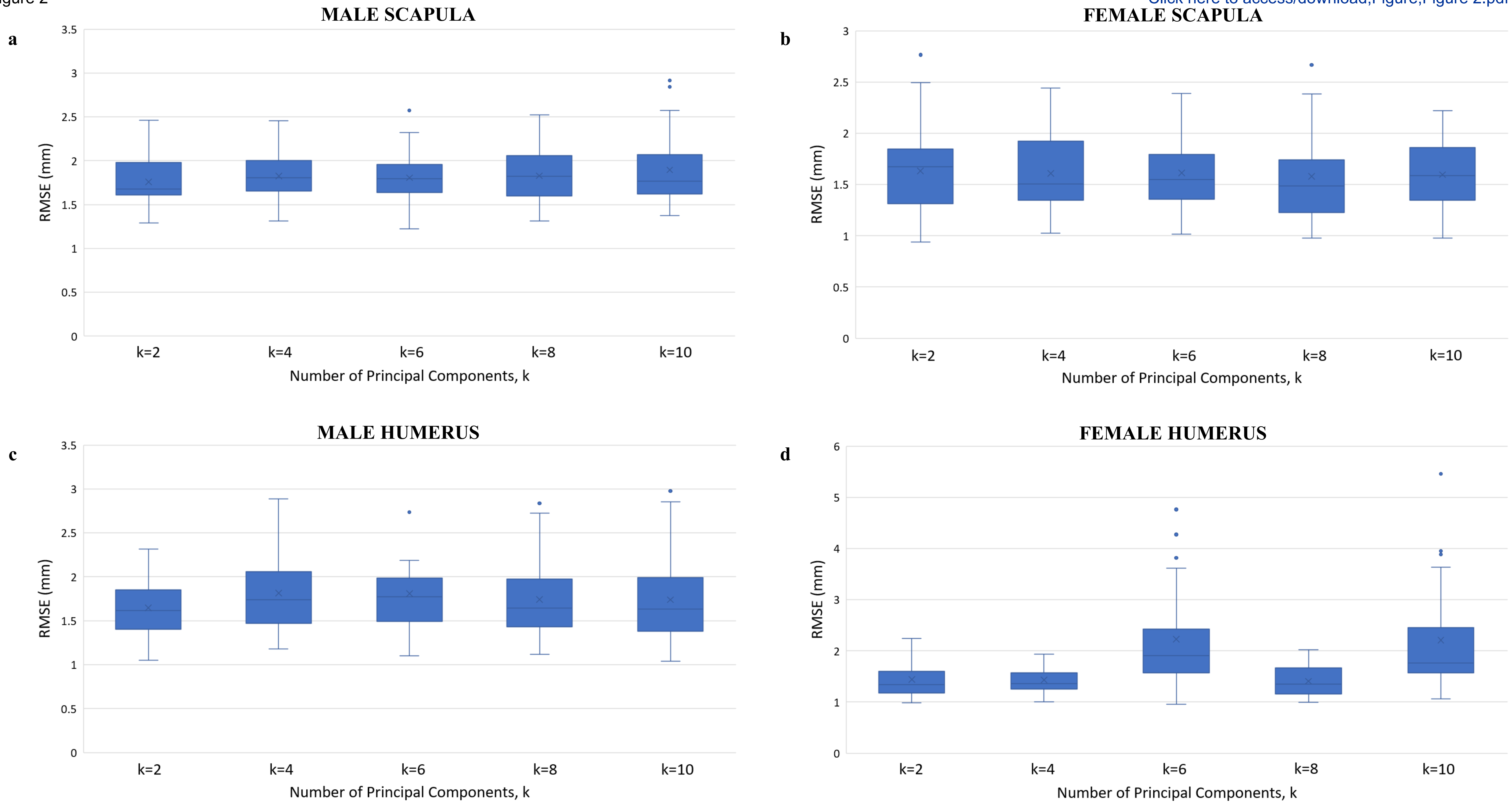
MALE SCAPULA
a
RMSE (mm)
0
0.5
1
1.5
2
2.5
3
3.5
k=2
k=4
k=6
k=8
k=10
Number of Principal Components, k
FEMALE SCAPULA
b
RMSE (mm)
0
0.5
1
1.5
2
2.5
3
k=2
k=4
k=6
k=8
k=10
Number of Principal Components, k
MALE HUMERUS
c
RMSE (mm)
0
0.5
1
1.5
2
2.5
3
3.5
k=2
k=4
k=6
k=8
k=10
Number of Principal Components, k
FEMALE HUMERUS
d
RMSE (mm)
0
1
2
3
4
5
6
k=2
k=4
k=6
k=8
k=10
Number of Principal Components, k

Figure 3

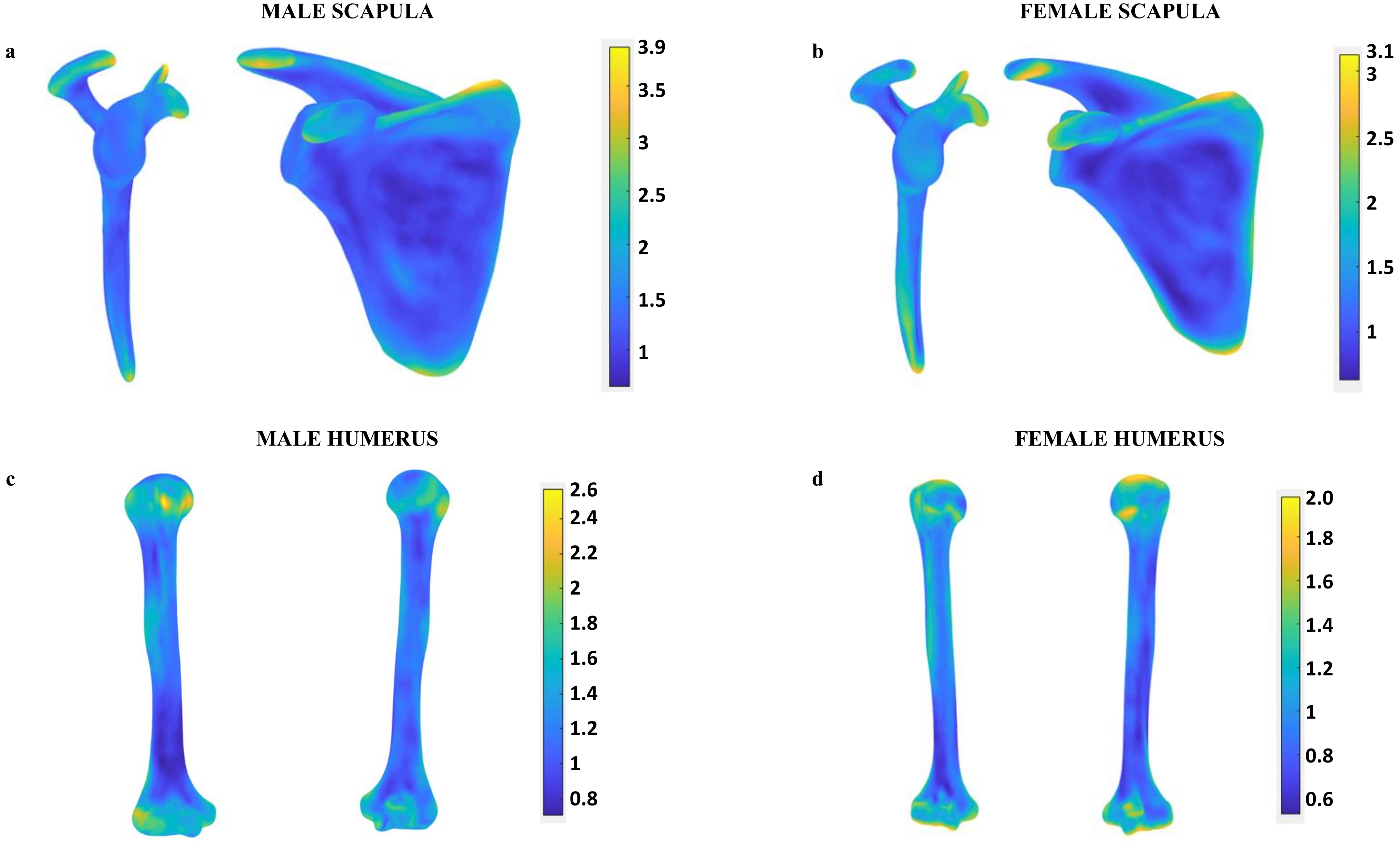
MALE SCAPULA
a
3.9
3.5
3
2.5
2
1.5
1
FEMALE SCAPULA
b
3.1
3
2.5
2
1.5
1
MALE HUMERUS
c
2.6
2.4
2.2
2
1.8
1.6
1.4
1.2
1
0.8
FEMALE HUMERUS
d
2.0
1.8
1.6
1.4
1.2
1
0.8
0.6

Figure 4

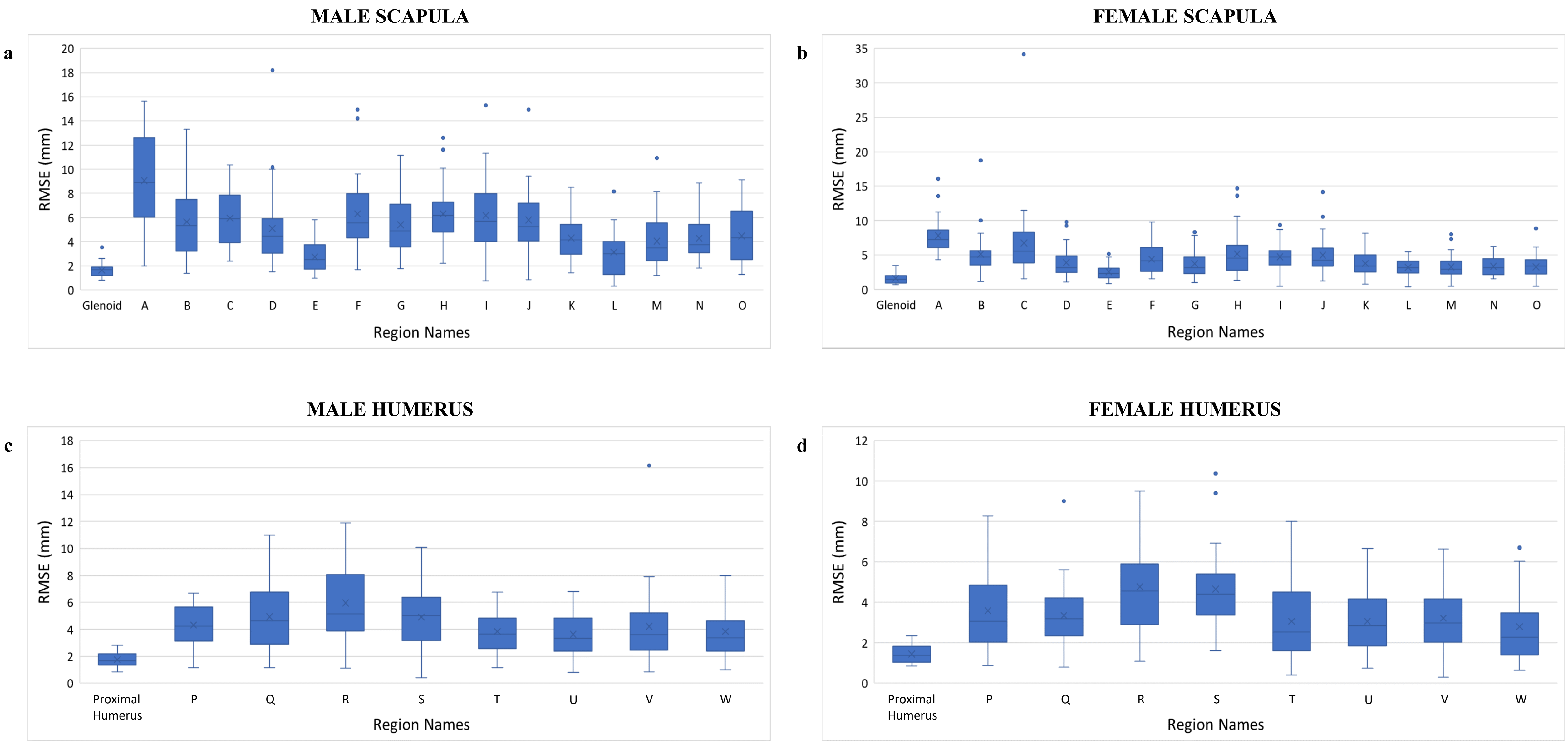
MALE SCAPULA
a
RMSE (mm)
0
2
4
6
8
10
12
14
16
18
20
Glenoid
A
B
C
D
E
F
G
H
I
J
K
L
M
N
O
Region Names
FEMALE SCAPULA
b
RMSE (mm)
0
5
10
15
20
25
30
35
Glenoid
A
B
C
D
E
F
G
H
I
J
K
L
M
N
O
Region Names
MALE HUMERUS
c
RMSE (mm)
0
2
4
6
8
10
12
14
16
18
Proximal Humerus
P
Q
R
S
T
U
V
W
Region Names
FEMALE HUMERUS
d
RMSE (mm)
0
2
4
6
8
10
12
Proximal Humerus
P
Q
R
S
T
U
V
W
Region Names

Figure 5

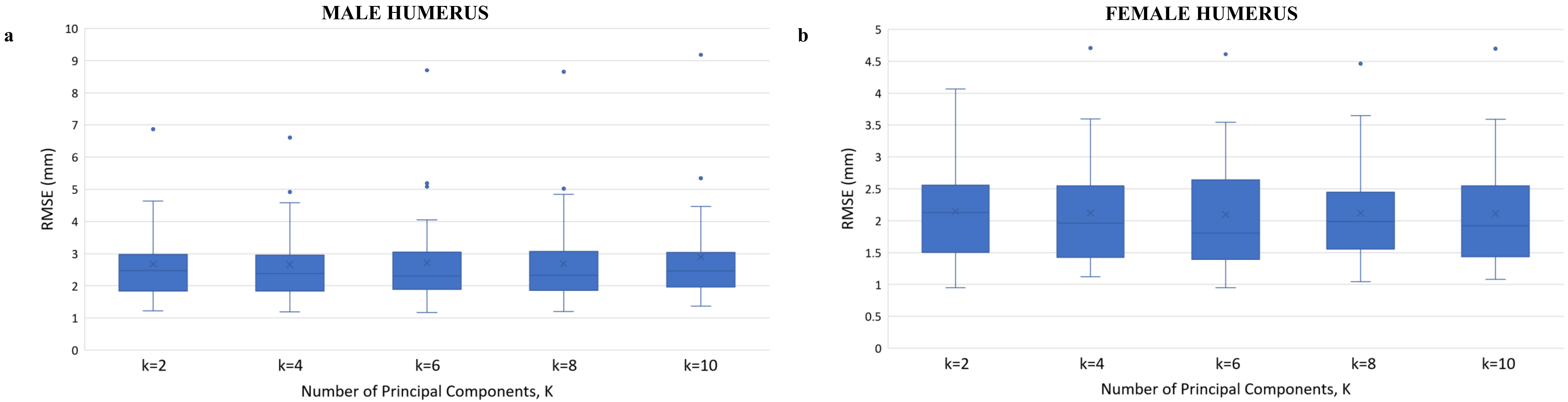
MALE HUMERUS
a
10
9
8
7
6
5
4
3
2
1
0
RMSE (mm)
k=2
k=4
k=6
k=8
k=10
Number of Principal Components, K
FEMALE HUMERUS
b
5
4.5
4
3.5
3
2.5
2
1.5
1
0.5
0
RMSE (mm)
k=2
k=4
k=6
k=8
k=10
Number of Principal Components, K

Figure 6

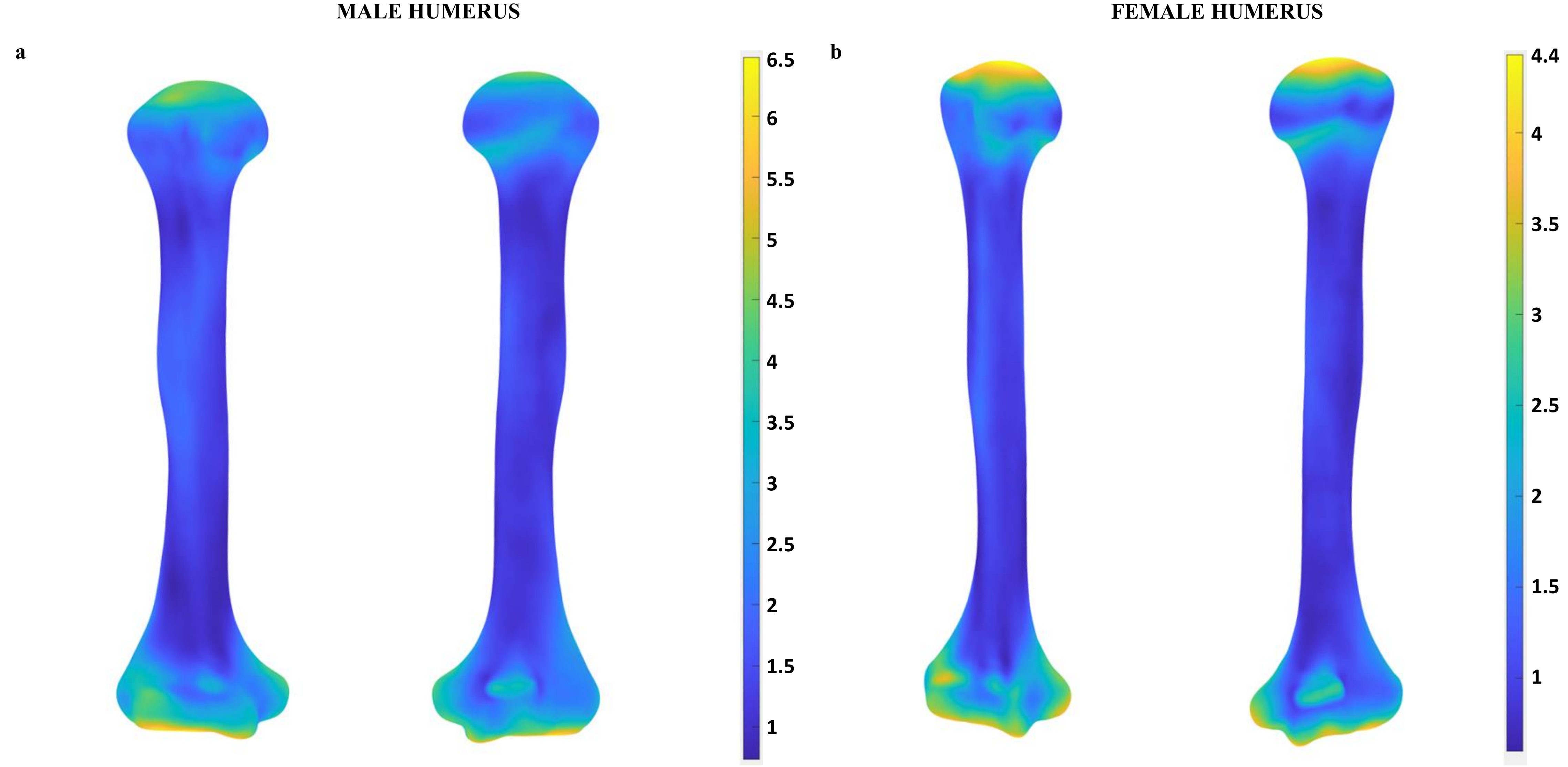
MALE HUMERUS
FEMALE HUMERUS
a
b
6.5
6
5.5
5
4.5
4
3.5
3
2.5
2
1.5
1
4.4
4
3.5
3
2.5
2
1.5
1

Figure 7

Click here to access/download;Figure;Figure 7.pdf

MALE HUMERUS

a

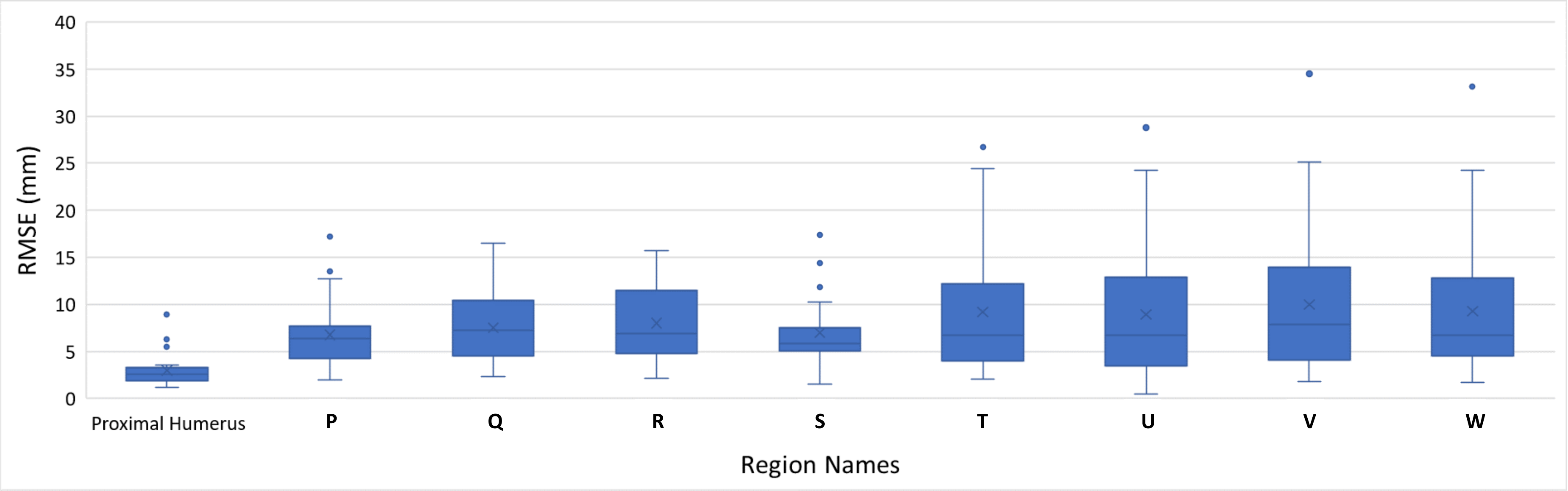

FEMALE HUMERUS

b

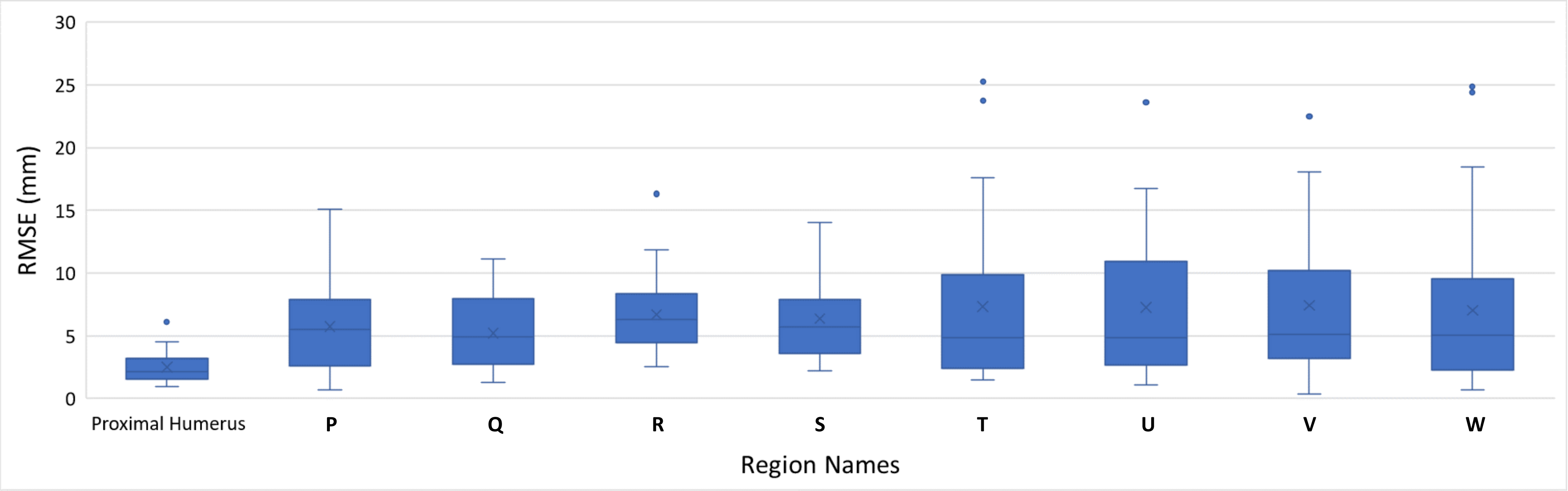

Table 1: Description of anatomical scapular landmarks used in shape prediction

Anatomical Landmark	Description
A	Superior angle
B	Medial edge of the scapula where the scapular spine meets the scapular body
C	Inferior angle
D	Base of the suprascapular notch
E	Most medial point of the spinoglenoid notch
F	Centroid of the lateral aspect of the acromion
G	Centroid of the medial aspect of the acromion
H	Centroid of the anterior aspect of the acromion
I	Centroid of the posterior aspect of the acromion
J	Tip of the coracoid
K	Point at which the coracoid angulates inferiorly
L	Superior rim of the glenoid
M	Inferior rim of the glenoid
N	Anterior rim of the glenoid
O	Posterior rim of the glenoid

Table 2: Description of anatomical humeral landmarks used in shape prediction

Anatomical Landmark	Description
P*	Most lateral point of the outline of the subscapularis insertion
Q*	Most medial point of the articular perimeter of the proximal humerus
R*	Most medial point of the outline of the supraspinatus insertion
S*	Most anterolateral point of the outline of the supraspinatus insertion
T	The most medial point of the medial epicondyle
U	The incision point between the medial epicondyle and medial part of the trochlea
V	The most inferior point of the medial trochlea
W	The most lateral point of the lateral epicondyle

* Landmarks on proximal humerus.